



Development of an automatic sorting robot for construction and demolition waste

Wen Xiao¹ · Jianhong Yang¹ · Huaiying Fang¹ · Jianguo Zhuang¹ · Yuedong Ku¹ · Xiaojun Zhang²

Received: 8 January 2020 / Accepted: 11 August 2020 / Published online: 28 August 2020
© Springer-Verlag GmbH Germany, part of Springer Nature 2020

Abstract

An automatic sorting robot is designed in this report. The system makes use of height maps and near-infrared (NIR) hyperspectral images to locate the ROI of objects and to do online statistic pixel-based classification in contours. This approach has two advantages: (1) to generate training data for sorting without manual work; (2) to get more stable final result. Two kind of features in hyperspectral image were extracted, a scale-sensitive algorithm was used to identify amplitude feature and a scale-insensitive algorithm was used to identify trend feature. After location and classification, the robot grabs valuable targets based on their position and posture and places them into the corresponding recycling area based on their category. The prototype machine can automatically sort construction and demolition waste (C&DW) with a size range of 0.05–0.5 m. The sorting efficiency can reach 2028 picks/h, and the online recognition accuracy nearly reaches 100%.

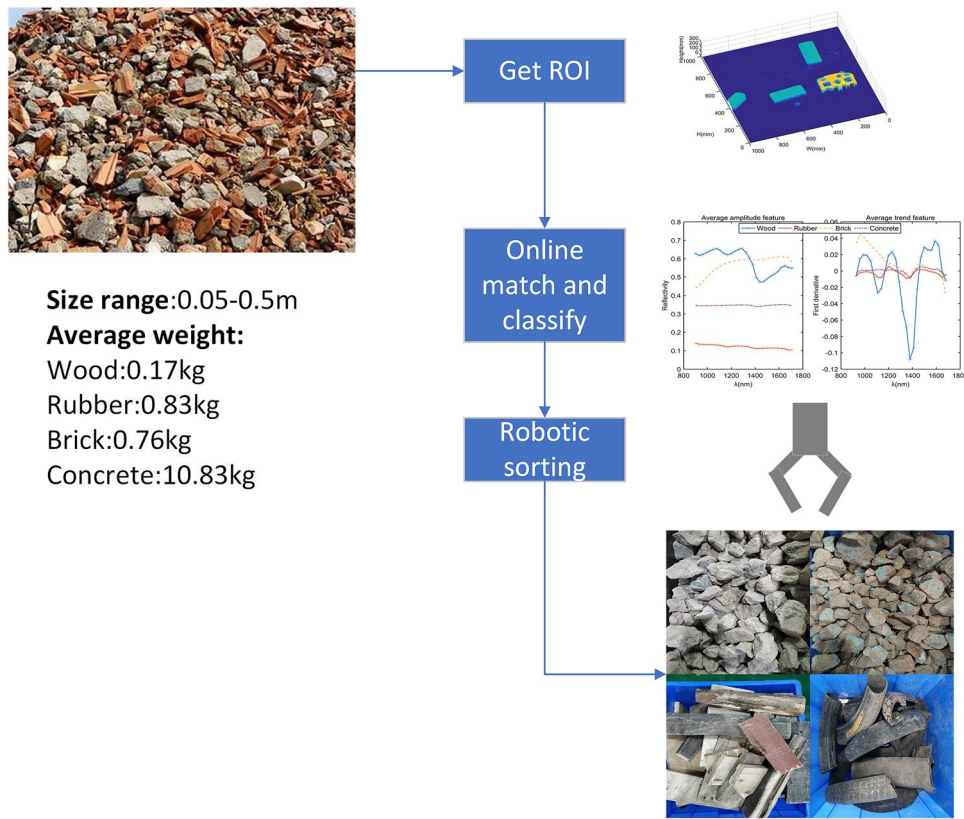
Electronic supplementary material The online version of this article (<https://doi.org/10.1007/s10098-020-01922-y>) contains supplementary material, which is available to authorized users.

✉ Jianhong Yang
yjhong@hqu.edu.cn

¹ College of Mechanical Engineering and Automation,
Huaqiao University, Xiamen, Fujian Province, China

² Fujian South Highway Machinery Co., Ltd, Quanzhou,
Fujian Province, China

Graphic abstract



Keywords Construction and demolition waste sorting · Automatic sorting robot · Height map detection · Hyperspectral image classification

Introduction

Construction and demolition waste (C&DW) production is increasing. Its uncontrolled generation and disposal negatively impact the environment, and thus research on methods that can recycle C&DW is becoming increasingly important. In China, C&DW production accounts for 30–40% of total waste production. Currently, the vast majority of C&DW is dumped, with an average recycling rate of only about 5% (Huang et al. 2018).

Traditional methods to process C&DW

Traditional methods of C&DW treatment cannot keep up with the pace of waste production today, and thus new treatment methods are required. In the traditional methods, C&DW must first be crushed several times, which is a prerequisite step for all subsequent processing (Chen and He 2018). After multiple mechanical screenings, the C&DW is manually sorted by hand, especially in low-income countries (Cesetti and Nicolosi 2016). This traditional type of

processing is complicated, inefficient, and expensive. Some C&DW can be effectively separated using methods based on a mechanism measuring density or magnetism (Ulsen et al. 2013). However, materials that are able to be sorted using such methods are limited. Most traditional methods, such as magnetic separation, pneumatic separation, hydraulic separation, and gravity separation, rely on some physical properties of the material for screening. These methods do not require a detection function and have a simple structure with high efficiency. However, it is difficult to separate some materials that have similar densities using just a simple preliminary separation, and the application range for density-based separation is limited. While C&DW comprises many different kinds of materials, the three most prevalent by volume are concrete, brick/block, and mortar. These materials are difficult to separate using traditional methods. In many cases, a pile of C&DW that is processed via traditional methods simply becomes another pile of C&DW in the end. Unseparated brick, concrete, and high-density wood can only be broken up into subgrades, resulting in relatively low-value material.

State-of-the-art methods to process C&DW

Sarc et al. (2019) summarized some of the latest methods used to process C&DW. According to their extensive investigation, digitalization and robotics in waste disposal are rapidly developing. The combination of sensors (mostly digital image) and large amounts of data can effectively improve the disposal capacity of waste. In fact, research has been conducted on the use of images to help sort waste such as ceramics and concrete (Gomes and Lima 2010). While this low-cost and simple method may succeed under simple working conditions, it may not be accurate or stable enough to operate well in actual C&DW processing plants. As deep learning technology has developed, so too has image classification technology, which has been used in many fields, including C&DW classification. Toğuçar et al. (2020) used an auto-encoder network with an integrated feature selection method to classify waste in convolutional neural network models, for which the most successful classification accuracy was 99.95%. Furthermore, region-based convolutional neural networks (R-CNNs) have offered a more in-depth learning method, specifically for the detection of the category and size of e-waste constituents (the classification accuracy of which ranged from 90 to 97%; Nowakowski and Pamuta 2020). The use of image classification technology based on deep learning significantly reduces the cost of the sensors, but due to the longer run times required, its use increases the difficulty of launching to online applications. Furthermore, this technology cannot attain a high accuracy without the inclusion of numerous labeled data, which is very expensive. Digital images contain low-level semantic information, which is why we recommend designing deeper networks to mine more useful information for classification.

Indeed, there are some sensors that can mine more information, which can be used for classification, such as hyperspectral image and thermal image. Rich information requires the use of simpler recognition methods and has fewer data requirements. It also results in reduced manual labeled costs. Near-infrared (NIR) hyperspectral images are widely used in material classification. In the NIR spectrum, the intensity of NIR light reflected from the surface of the material to the lens is recorded. The functional groups in organic molecules (such as -OH, -NH, -CH, and -SH) absorb certain bands of light in the NIR region. The reflectivity of a material containing such functional groups thus has obvious characteristics (Cesetti and Nicolosi 2016); e.g., organics such as wood and plastic have obvious features in the NIR waveband region. Contaminants such as plastics and wood preservatives can be identified by NIR hyperspectral imaging, and data collected from these laboratory experiments can be transferred to small-scale industrial operations (Mauruschat et al. 2016). Serranti et al. (2012) used images within the wavelength range 900–1700 nm to classify plastic. Their

recognition result could tolerate the changes in color and density, but the black samples were ignored because of their weak reflectance properties. Wu et al. (2020) realized a plastic classification accuracy of more than 99%, and designed an automatic sorting system for large plastic segments. In recent studies, material classification has been the first step, always with the end goal of automatic sorting. Wood and plastic are both organic materials and have obvious features in the NIR spectral region, so it is easy to identify clean samples. However, the inorganics in C&DW, such as concrete, brick, and stone, are more valuable, because they can be recycled and used as building materials (Paranhos et al. 2016). The reflectivities of the inorganics are relatively uniform, which is one of the major difficulties in analyzing their spectral recognition. Thermal imaging has been used to classify a variety of materials with high accuracy (Paulraj et al. 2017). However, before classification, the materials must be grouped into categories, such as plastic and paper. This requirement is unable to be met in C&DW sorting. In summary, digital imaging can be used to classify most waste when the amount of data with labels is high enough, but the long running time presents a significant problem. Moreover, NIR hyperspectral images have much richer information, and their classification is pixel-based. However, digital image classification is picture-based, which makes the NIR hyperspectral data and labels easy to produce. However, the capability to identify inorganic materials needs to be improved. The images out of the NIR range are not mature enough for material identification.

After classification, how to sort the object is also an essential problem to solve. Only when these two processes are combined will they be practical for sorting C&DW. Paulraj et al. (2016) designed a system for household garbage (aluminum cans, plastic bottles, and tetra packs) equipped with a thermal imaging camera, a proximity sensor, and a 5-DOF robotic arm. This setup obtained a classification rate of 94.3%. An intelligent waste sorting system with a robotic arm was reliable and achieved an accuracy of about 82% for the categorization of 11 (waste) objects of different sizes and types (Diya et al. 2018). While robotic arms are a well-developed technology, most are not suitable for grabbing heavy objects, or they are too expensive. Kujala et al. (2016) designed a truss-type robot for sorting C&DW based on classes determined by color. Such truss-type robots can handle heavy objects, and their operational control algorithm is easy to design. In addition to these vision-based robots, a soft sensorized robotic gripper that is fully electrically driven and can detect the difference between paper, metal, and plastic should be employed. The classification accuracy of this system can reach 85%. This classifier works over a variety of objects, including those that would fool a purely vision-based system (Chin et al. 2019).

NIR hyperspectral imaging is used in this paper to classify C&DW. In order to improve the identification ability and stability, pixel-based classification is realized by two methods: (1) an amplitude feature and scale-sensitive algorithm, and (2) a trend feature and scale-insensitive algorithm. We combine two sets of identification results to eliminate uncertain pixels and, according to the ROI obtained from the height map, to statistically choose certain pixels that will result in selecting the appropriate object. Then, a simple truss-type robotic is designed to automatically classify objects. The labels of the data do not need manual marks, and the accuracy of online recognition nearly reaches 100% (There is no incorrect classification in the online experiment.) The paper is structured as follows: “[Experimental materials and equipment](#)” section describes the experimental materials and equipment. “[Methodology for automatic online sorting](#)” section describes the entire procedure of designing the robotic system, and “[Material identification](#)” section describes the classification method. “[Target detection based on height map](#)” section discusses the ROI extraction result according to the height map, while “[Feature extraction](#)” section discusses the hyperspectral feature extraction result. “[Offline classification](#)” section discusses the offline classification results, and “[Classification results of online matching and identification](#)” section discusses the results of the online matching and identification. “[Online sorting accuracy and efficiency](#)” section discusses the accuracy and efficiency of online sorting, and finally, “[Conclusions](#)” section draws the conclusions.

Materials and methods

Experimental materials and equipment

As shown in Fig. 1, the robotic system can be divided into four modules: (1) a main conveyor, which includes an adjustable-speed conveyor, (2) a detection module, which includes a 3D camera (LMI Gocator 2880) and an NIR hyperspectral camera (Specim FX17E, wavelength range 900–1700 nm; number of bands: 224), (3) a light source module, which includes a dome light source for the hyperspectral camera, and (4) a manipulator, which includes a four-axis truss-type robot for sorting the material of interest from the waste stream. The control system of the robot is Beckhoff CX2040.

Some samples used in our experiment are shown in Fig. 2. During the training process one specified and known category of objects was analyzed each time; first the height map is used to eliminate the background, then the ROI was labeled as pre-specified category. The smallest object was about 25×25 pixels in the hyperspectral image, and at least 625 data points with labels were produced with the pixel-based classification method. For each class, 5000 pixels (10

pixels \times 500 objects) were randomly selected as the training set. Because of a problem in the manufacturing process, a few black bricks were mixed in with the normal bricks. After random selection was applied to the training set, relatively few black bricks remained; so another 1000 pixels (10 pixels \times 100 objects) of black brick were added to the brick data. For each class, 2000 pixels (10 pixels \times 200 objects) were selected as the testing set. Because this paper focuses on C&DW, four common C&DW materials that are difficult to separate using traditional methods were selected, namely wood, rubber, brick, and concrete. These samples were sourced from construction sites. Before classification, the samples were crushed and cut to obtain objects within a size range 0.05–0.5 m. The average weights of the materials are as follows: wood is 0.17 kg/piece, rubber is 0.83 kg/piece, brick is 0.76 kg/piece, and concrete is 10.83 kg/piece. The robot hand used in this study is specialized for objects with a minimum size of 0.05 m. A pneumatic valve can be used in further studies to process particles smaller than 0.05 m.

Methodology for automatic online sorting

The overall flow of the proposed method for an automatic sorting robot is shown in Fig. 3. At construction/demolition sites, there is a lot of dust on the surface of the conveyor belt, making it difficult to obtain accurate position and contour information using a 2D camera. The 3D contour of an object and its position and posture can be accurately extracted from the height map. After the height map is obtained, a timeline is established for each contour (T_0 = current time). Based on the speed of the conveyor belt, the position of the target can be tracked in real time. At T_0 , the obtained height map is processed to collect all of the contours in the image, and the position and posture are obtained from the contours and stored. At T_1 , all pixels within each contour in the field of view are identified as the target contour enters the hyperspectral field of view. At T_2 , the target contour is completely out of the hyperspectral field of view; that is, all of the pixels in the contour have been recognized. Then, the recognition results for all pixels in the contour are counted, and the target is judged to be in the category with the highest proportion of recognition results. At T_3 , the target enters the sorting range. The robot determines whether or not to grab the target based on its category. If so, the robot grabs the target according to the position and posture obtained at T_1 and then places it into the recycling area of the corresponding category. Otherwise, the target is ignored.

The object height is acquired using the 3D camera in the line-scanning mode. For each frame, the height of one line in the field of view of the camera is acquired. The overall height information is obtained by combining multiple frames. The value of a pixel in the height map indicates the height of the object at the corresponding position. After

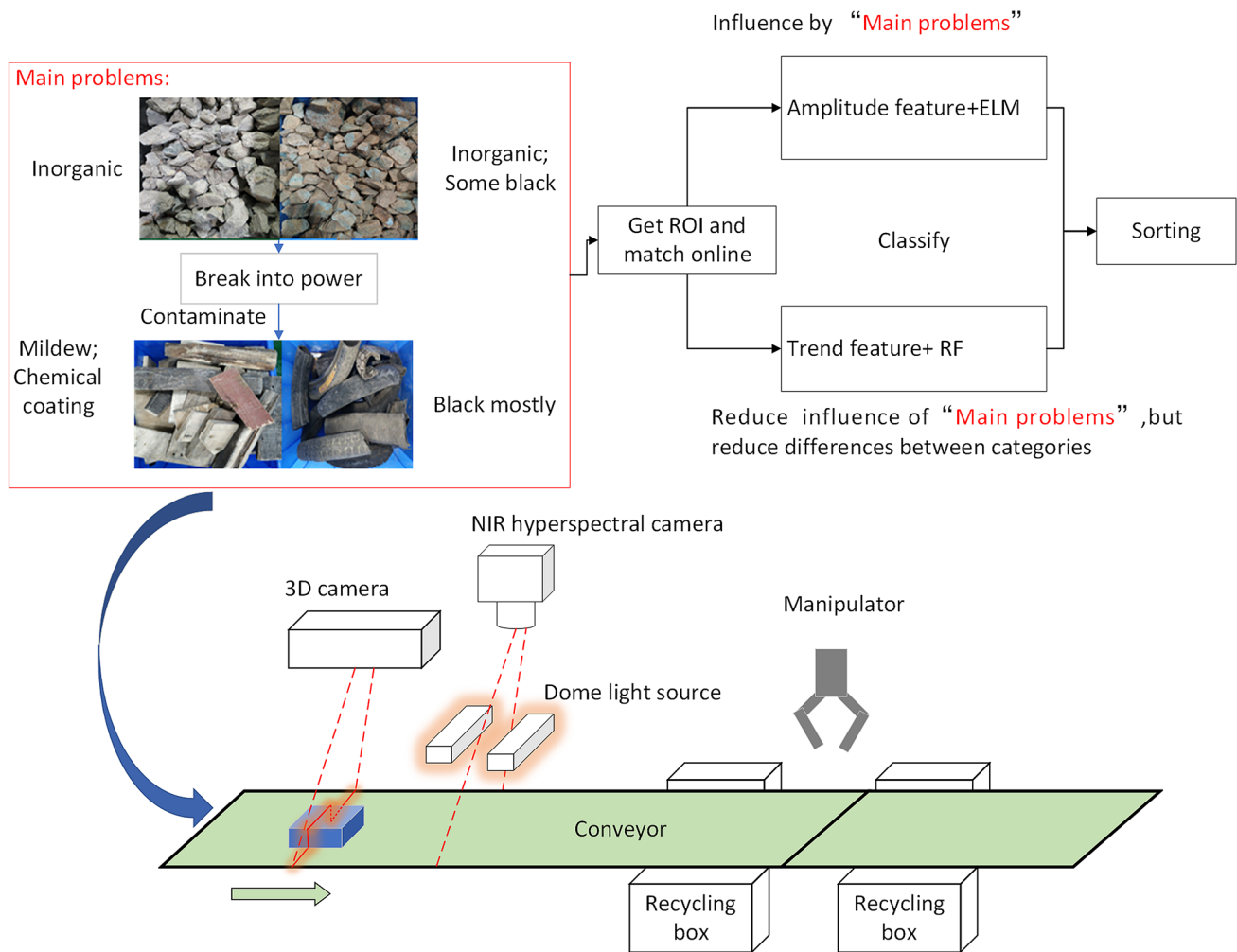


Fig. 1 Schematic diagram of prototype robotic system. The 3D camera is the LMI Gocator 2880. The NIR hyperspectral camera is the Specim FX17e. The dome light source emits light to the dome coat-

ing via Teflon, which is then reflected to the object's surface. The Manipulator is a truss-type robot designed by the authors

calibration, the height of the belt was zero. Therefore, even if the conveyor contained a lot of dust, the exact contour of the object could be extracted. The steps for target detection and tracking are described below.

The conveyor speed is v (m/s), the distance between the 3D camera field of view and the hyperspectral camera field of view on the y -axis is D_1 , and the distance between the field of view of the hyperspectral camera and the starting point of the sorting range is D_2 . The calibration factor of the 3D camera is H_c (mm/pixel), and the calibration factor of the hyperspectral camera is S_c (mm/pixel). The physical coordinate system and the 3D camera coordinate system are shown in Fig. 3.

Step 1 For each $H/3$ frame, collect an image combined with the latest H frames and record the current time (T_0), where the size of each processed image is $W \times H$.

Step 2 Binarize the height map with a threshold of 5 mm (i.e., pixels with heights lower than 5 mm are ignored). Find the contours, excluding contours for which the width of the minimum enclosing rectangle is less than 5 mm.

Step 3 Extract the first point of the contour, $FP = (x_0, y_0)$ (in height map coordinates), and calculate its real position (X_0, Y_0) in the physical coordinate system as:

$$(X_0, Y_0) = (x_0 \times H_c, (H - y_0) \times H_c). \quad (1)$$

Assuming that the contour starts from the first point and the total span is M frames for a 3D image, the start and end points of the contour of each frame on the x -axis are, respectively, B_i and E_i , where $i \in [0, M - 1]$. The center of the minimum enclosing rectangle $P = (x_c, y_c)$ is set as the center of the object. (X_c, Y_c) can be obtained using Eq. (1).

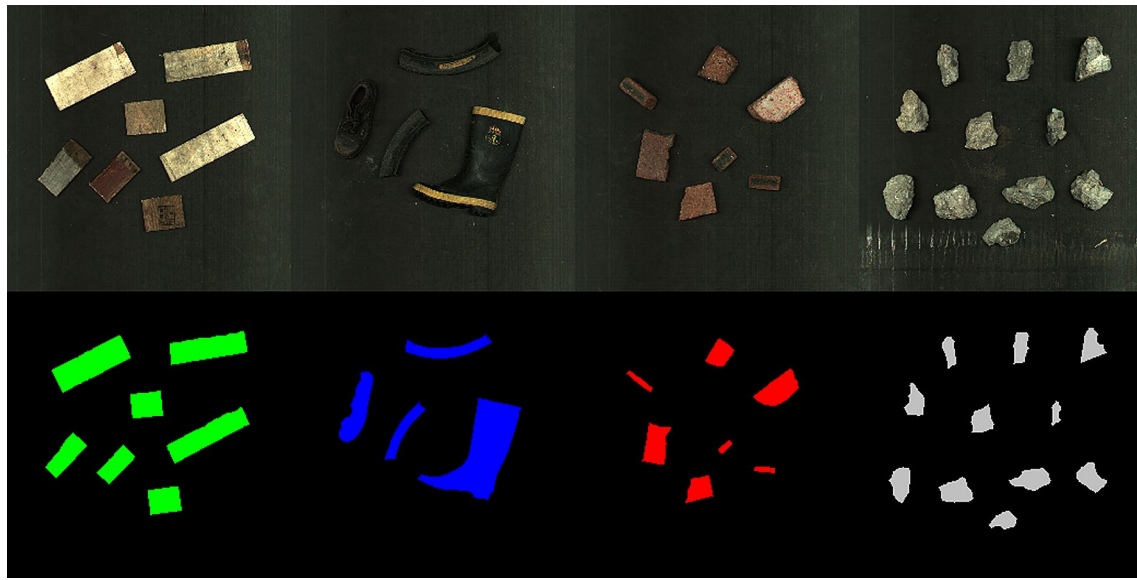


Fig. 2 Photographs of some samples and their corresponding color labels. Green, blue, red, and gray indicate category 1 (wood), category 2 (rubber), category 3 (brick), and category 4 (concrete), respectively

The angle between the long axis of the minimum enclosing rectangle and the positive direction of the y-axis of the physical coordinate system is the target angle A , which is positive in the counterclockwise direction and negative in the clockwise direction.

Step 4 Refresh the current location of the first point of the target every 10 ms as $(X_{0t}, Y_{0t}) = (X_0, Y_0 + v * (t - T0))$. When $Y_{0t} \geq D1$, the outline of the frame m is identified, where $m = \text{int}[(Y_{0t} - D1)/H_c], m \in [0, M - 1]$. The current contour corresponding to the range of pixels in the hyperspectral image is $\left[\text{int}\left(B_m \times \frac{H_c}{S_c}\right), \text{int}\left(E_m \times \frac{H_c}{S_c}\right) \right]$.

Step 5 When $m = M - 1$, the target is completely out of the hyperspectral field of view. At this time ($T2$), the identification of all pixels in the target contour is complete. Count all of the recognition results, and place the target in category C with the highest proportion of recognition results. If category C is a category that needs to be sorted, proceed to step 6; otherwise, ignore the target.
Step 6 Refresh the center point of the target every 10 ms as $(X_{ct}, Y_{ct}) = (X_c, Y_c + v * (t - T0))$. When $Y_{0t} \geq D1 + D2$, control the robot to grab the object at coordinates (X_{ct}, Y_{ct}) . When the robot is moving, (X_{ct}, Y_{ct}) is still refreshing every 10 ms to keep the theoretical position error between the robot and object less than $10 * v$ mm ($v = 0.25$ m/s in the experiment). The rotation angle of the grab posture is A . Control the robot to place the object into the recycling box corresponding to category C .

Material identification

A previous study showed that an extreme learning machine (ELM) is suitable for identifying the amplitude characteristics of a spectral curve due to its sigmoid activate function. The study additionally showed that random forest (RF) is suitable for identifying the trend characteristics (Xiao et al. 2019). The Haar wavelet transform (HWT) is used to extract the characteristic reflectivity R , which is used for identification by ELM. For online recognition, the reflectivity of each pixel and its trend feature are, respectively, identified. For each pixel, two recognition results are obtained. The reflectivity curve is related to the material properties, surface texture, and color of the object. To avoid the influence of the uneven light source intensity and the dark current in the camera, the reflectivity must be calibrated first. The calibration formula is:

$$r = (D - D_B) / (D_W - D_B) \quad (2)$$

where D_B is the standard dark frame, which can be captured by covering the lens cap, D_W is the standard white frame, which is taken using a standard white board made of Teflon with a reflectivity of 99%, D is the original data, and r is the reflectivity after calibration.

Feature extraction

Because of the high spectral resolution, the correlation between adjacent bands is strong, which results in high

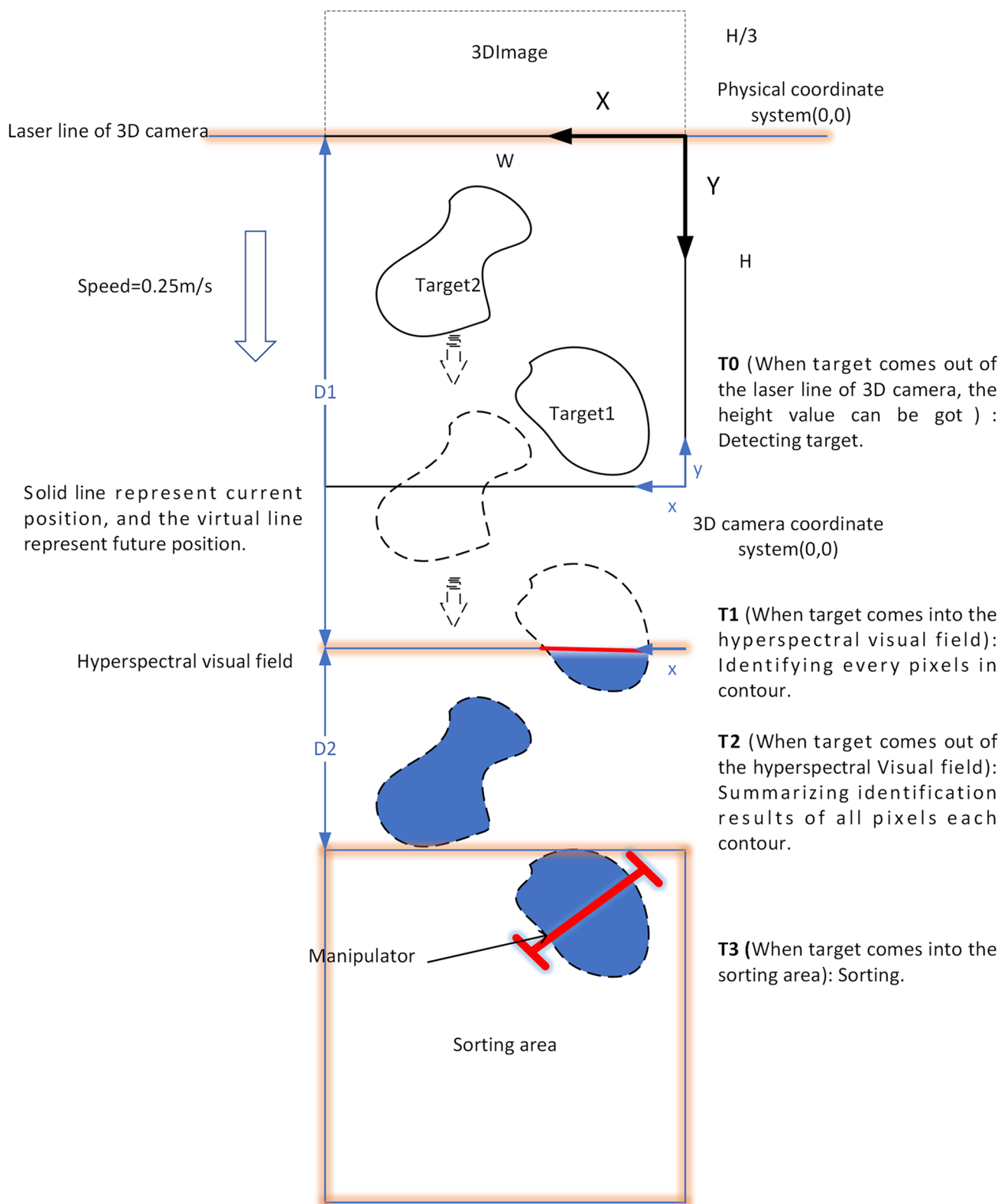


Fig. 3 Procedure for online automatic sorting

data redundancy. To improve the efficiency of the data processing, it is necessary to compress the reflectance data, for which the HWT is used in addition to extracting features. The reflectivity (r) is the input, and the characteristic reflectivity (R) is the output. Equation (3) is executed three times; each time, the dimension of the input data is reduced by half. The final dimension of the output data is $\frac{224(\text{Input dimension})}{2^3(\text{executed 3 times})} = 28$,

$$R_i = \frac{r_{2i} + r_{2i-1}}{2} \begin{cases} i \in (0 \sim k/2 - 1) & \text{if } k \text{ is odd} \\ i \in (0 \sim (k-1)/2 - 1) & \text{if } k \text{ is even} \end{cases} \quad (3)$$

where k is the dimension of the input data. The feature R is the amplitude, which is influenced by the surface color. Different samples of a given material will thus have different features. To improve identification stability, the first derivative (FD) of R is obtained using Eq. (4). The FD indicates the trend feature. Equation (4) can be replaced by Eq. (5) because the spectral resolution is constant. Due to the edge effect, the dimension of the FD is the characteristic reflectance dimension minus 2 (i.e., $28 - 2 = 26$).

$$\text{FD}_i = (R_{i+1} - R_{i-1}) / (\lambda_{i+1} - \lambda_{i-1}) \quad (4)$$

$$\text{FD}_i = R_{i+1} - R_{i-1} \quad (5)$$

Identification algorithm

Two algorithms are used for identification, namely ELM and RF. ELM is a single-hidden-layer feed-forward neural network. The algorithm does not need to adjust parameters through error back-propagation, and ELM is a scale-sensitive method due to its sigmoid active function. It obtains the parameters with the smallest theoretical error by solving the matrix equation. Therefore, the algorithm has a fast training speed and high efficiency. With a sufficient number of hidden layer nodes, any complex function can be fitted theoretically (Huang 2014). RF is a strong classifier composed of multiple weak classifiers. Two random selections are used to improve identification ability. Some subsets are first randomly selected from the training samples, and then some sub-features are randomly selected from the subsets. The sub-features and corresponding subsets are used to train the Classification and Regression Tree (CART) algorithm (Rutkowski et al. 2014), which is a scale-insensitive method because the split principle of CART is to find a best split feature and best split node that are not influenced by feature scale. The final result is obtained by combining the results of all classification trees.

Results and discussion

Target detection based on height map

As shown in Fig. 4, it is difficult to distinguish a target on a dust-covered conveyor in color images. An incorrect contour will greatly influence the accuracy of identification and sorting. The height map can clearly separate the target from the background. To ignore the height fluctuation of the conveyor and the influence of the dust, the height threshold is set to 5 mm. The contour is judged to be valid when the height value exceeds the threshold. The target is extracted accurately by processing the height map. This ensures accurate recognition and grasping of the target.

Feature extraction

The reflectance curves of some samples are shown in Fig. 5a, and the corresponding average characteristic reflectivity (amplitude feature) and its FD (trend feature) are shown in Fig. 5b. Wood is an organic material with obvious absorption peaks. However, because of the influence of brick powder, moisture, mildew, and chemical coating, the amplitudes and trends of different samples are quite different. These trends have two forms before 1400 nm, and the reflectance amplitude span is large. For rubber that is not black, the curves have obvious trend characteristics, but the value is small, and the amplitude span is large. For black rubber, reflectivity is low, and there are no obvious features. In other words, the curves for rubber depend on color. For brick, although most curves do not have characteristic absorption peaks, they generally show a monotonous upward trend, and the amplitude is mainly concentrated between 0.4 and 0.7, its characteristics are obvious. However, the black bricks have a lower reflectance, and their curves are similar to those of black rubber. For concrete, the curves have a decreasing trend at around 1350 nm, but the variation range is relatively quite small. According to the reflectance curve, some of the samples for a given material are not identical, the amplitude

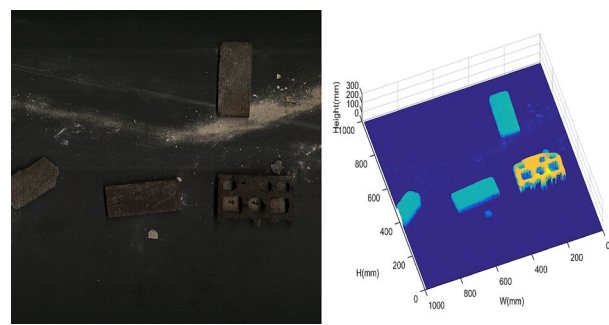


Fig. 4 Example of height map

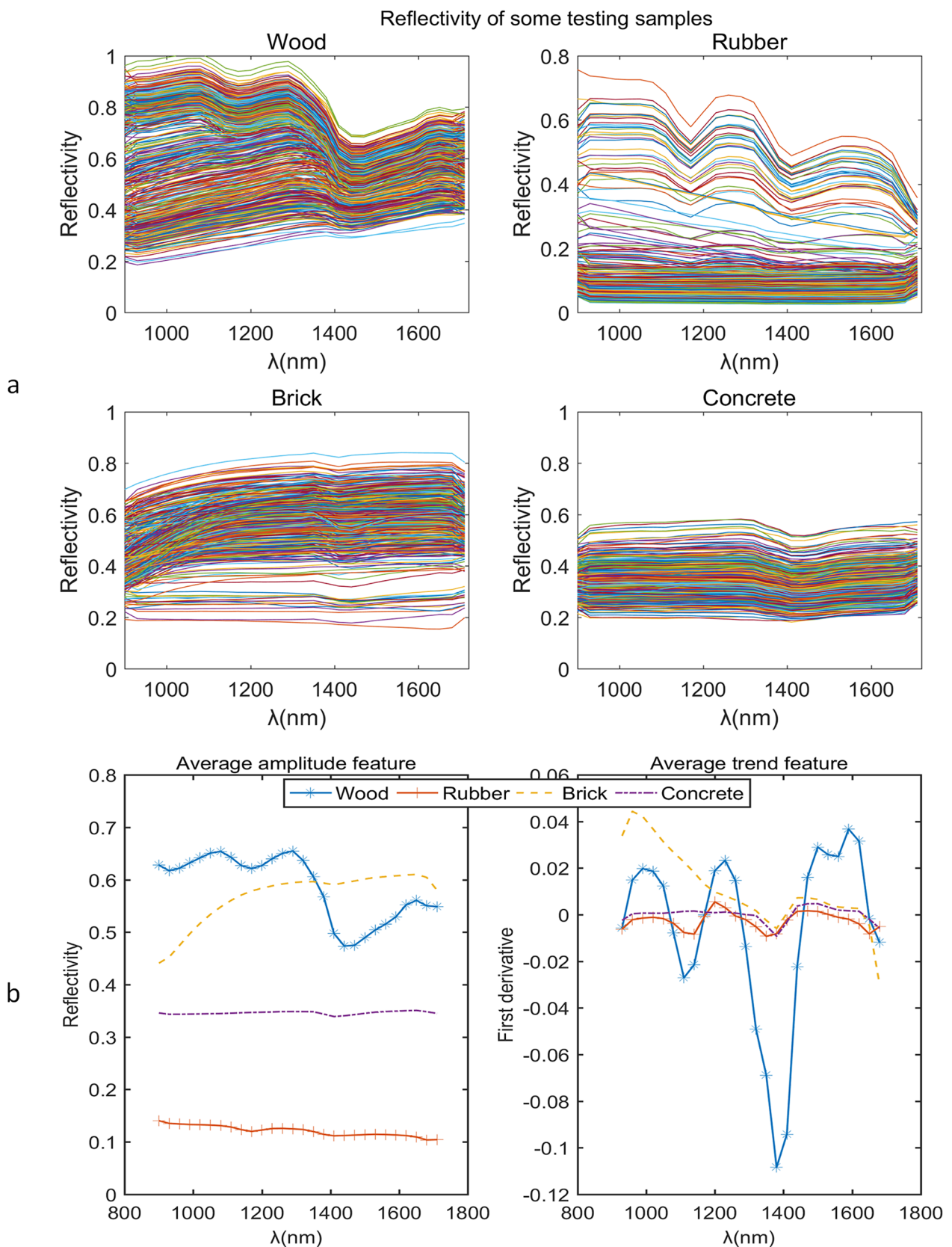


Fig. 5 **a** Reflectivity of various samples; **b** average characteristic reflectivity (left) and its first derivative (right)

span is large, and the trend characteristics take different forms. These factors can lead to errors in identification.

Offline classification

The confusion matrix of ELM for identifying the characteristic reflectivity is shown in Table 1. The confusion matrix shows the mutual misjudgment between categories as well as the precision and recall of each category. The recall of wood is the lowest. Because the initial wood used has obvious features, its reflectivity will change significantly when it is polluted by brick and concrete powder. At the same time, the moisture, mildew, and chemical coating will also change the reflectivity. The recall will improve when the training samples account for these negative influences. The mutual misjudgment probabilities for brick and rubber are similar, because both of them have black samples that absorb most light. Although the recall for wood is low, when wood is identified, the precision is 100% because the overall characteristics of wood are very distinguishable (i.e., no other types of material are misjudged as wood). The precision of brick is the lowest because brick is the most likely material to break into powder, which will contaminate other materials, resulting in some abnormal data results for the other types of materials. Although there are some flaws in each category, the overall identification accuracy for the four types of materials is 94.26%, indicating that they can be distinguished, but identification needs some improvement.

Table 1 Confusion matrix of ELM for identifying characteristic reflectivity

	True class				Total	Precision/%
	Wood	Rubber	Brick	Concrete		
<i>Identification class</i>						
Wood	1693	0	0	0	1693	100
Rubber	0	1923	54	0	1977	97.27
Brick	199	72	1936	11	2218	87.28
Concrete	108	5	10	1989	2112	94.18
Total	2000	2000	2000	2000	8000	
Recall/%	84.65	96.15	96.80	99.45		94.26

Table 2 Confusion matrix of RF for identifying first derivative of characteristic reflectivity

	True class				Total	Precision/%
	Wood	Rubber	Brick	Concrete		
<i>Identification class</i>						
Wood	1958	0	0	0	1958	100
Rubber	0	1888	72	32	1992	94.78
Brick	15	89	1928	3	2035	94.74
Concrete	27	23	0	1965	2015	97.52
Total	2000	2000	2000	2000	8000	
Recall/%	97.90	94.40	96.40	98.25		96.74

The results of using RF for identifying the FD of characteristic reflectivity are shown in Table 2. The overall identification accuracy is slightly improved, and the recognition performance for the various types of materials is relatively balanced. The identification method based on RF has a good overall performance. The method based on ELM has a higher recall than that of the method based on RF, except for wood. Consequently, the moisture, mildew, and chemical coating may be the primary influencers of the amplitude of reflectivity, and changes to trend feature are slight. The two methods have advantages and disadvantages. To improve the adaptability to complex conditions during online identification, the recognition results of the two methods can be combined. That is, there would be two recognition results (ELM + R and RF + FD) for each pixel, which can reduce the recognition errors caused by contaminants such as dust.

Classification results of online matching and identification

The identification results of online matching are shown in Fig. 6. The top, middle, and bottom panels show a pseudo-color image synthesized using a hyperspectral image of an actual sample and the recognition results obtained using ELM + R and RF + FD, respectively. The two recognition result maps are matched in real time with the contour of the height map. Only pixels with a height greater than 5 mm are identified. The black color in the figure is the background (pixels with a height lower than 5 mm), which

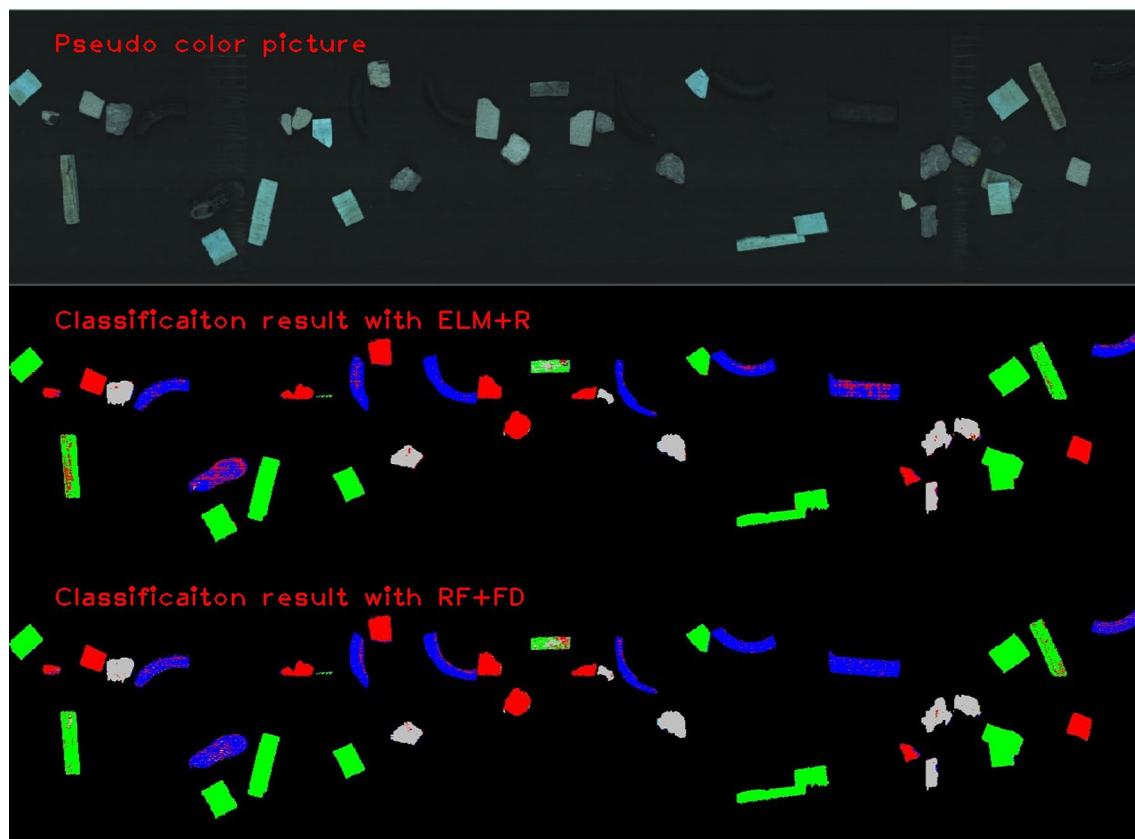


Fig. 6 Online classification results for ELM + R and RF + FD (black: background; green: wood; blue: rubber; red: brick; gray: concrete)

is not recognized. Green, blue, red, and gray pixel colors indicate that the recognition result for the corresponding pixel is wood, rubber, brick, and concrete, respectively. As shown in Fig. 6, some pixels are erroneously judged. However, when online classification is performed, the recognition results for the entire contour are counted, and the accuracy of online recognition reaches 100%. According to ROI from 3D contours, combining amplitude and trend feature can significantly improve the classification accuracy because both the quantity of detected pixels and the quality of every pixel increase.

Online sorting accuracy and efficiency

The online sorting accuracy and efficiency for a conveyor speed of 0.25 m/s are shown in Table 3. “Successful grabbing” shows the number of pieces of the given objects on the conveyor that were captured and placed into the sorting area. “Classification accuracy” shows the proportion of the given objects placed into the correct category sorting area. “Missing” shows the number of pieces of the given objects that exceeded the execution range of the robot. “Missing” is shown because we want to test the extreme efficiency of the robot, and in real industrial conditions, this situation

Table 3 Sorting accuracy and efficiency for fixed conveyor speed of 0.25 m/s

Group (2 min)	Samples (pieces)	Successful grabbing (pieces)	Classification accuracy (%)	Missing (pieces)
1	100	72	100	28
2	100	68	100	32
3	100	70	100	30
4	100	64	100	36
5	100	64	100	36
Successful grabbing efficiency	338/500=67.6%			
Average efficiency (picks/hour)		2028		

will also occur. Increasing the number of robots used in future studies can improve the efficiency and mostly avoid this problem. The classification accuracy of the test reached 100%. This can mainly be attributed to the numerous pixels detected and the combination of amplitude and trend feature for classification. In this test, the average sorting efficiency of the robot was 2028 picks/h, which reflects the average number of pieces successfully sorted (objects are grabbed and thrown into the correct sorting box) in an hour. Actual performance may vary slightly depending on the distribution of objects on the conveyor. The robot will lose samples when there are too many objects on the belt. This will greatly reduce the rate of grabs that are successfully sorted. The capture route and sequence in this work are not optimal, so there is room for efficiency improvement in future studies. On the other hand, it is easy to include additional robots in the setup and have them work together within one detection system. (Note that the Beckhoff system used in this study can control more than 300 axes at the same time.) A single robot takes responsibility for only one or two types of material. This will multiply the successful grabbing efficiency by a significant factor. In practice, one may choose to sort only valuable materials. For example, consider that only concrete is selected. Concrete has a density of about 2500 kg/m³. Using the average weight of concrete, the volume is then $2028 \times 10.83 = 21.96$ t/h. The volume with the largest size 0.5 m is then: $0.5 \times 0.5 \times 0.5 \times 2500 \times 2028 = 633.75$ t/h. (In real condition, this value will be smaller than 633 t, because it is not possible to produce particles with size 0.5*0.5*0.5). For a single robot working 24 h a day and 300 days per year and a target size of 0.05–0.5 m, at least 4560 (with minimal size) tons of concrete can be sorted in 1 year. (The processing capacity can reach about 146,000 t using the average weights of concrete in this study.)

The sorting results for the proposed method using an automatic robot are compared with those for a traditional method in Online Resource 1. The traditional method cannot separate materials finely with similar densities, such as concrete and brick, which account for most of C&DW. Mixed materials can only be used for pavement foundation and thus have low value. The proposed method for an automatic sorting robot can finely separate most C&DW. Cleanly separated waste is a valuable resource. Specifically, concrete can be crushed to make aggregate to substitute granules, which can reduce the exploitation of river sand, and brick can be used for pavement foundation. The classification test is shown in video (Online Resource 2), according the classification result, the online test of automatic sorting is shown in video (Online Resource 3). The video showed how the robot work in real sorting condition, it can fully automatic grab the object and throw it into corresponding recycling area according to the material category without human supervision. In the traditional craft to fine sorting C&DW,

the human sorting platform can be replaced with the robot designed in this paper. Robot can process heavier objects, so there is no need too much preprocessing. After classification, every category is executed corresponding post-processing. The concrete is most valuable in four materials studied in this paper, after peel-type crushing and counterattack crushing, recycled aggregates of different particle sizes showed in Online Resource 4 are produced.

Conclusions

This paper presented an automatic sorting robot system with the following key components: a 3D camera, an NIR hyperspectral camera, and a truss-type robot. The system is designed for C&DW, which can improve the resource utilization rate, achieve fine classification, and avoid environmental damage caused by inappropriate disposal processes. Due to the online matching of height maps and hyperspectral images, large amounts of data and labels can be easily obtained without the employment of manual marking. Combining multi-pixel classification results and ignoring uncertain pixels, the online accuracy reaches almost 100%. As the robot used in this study was designed by the authors for simple applications, the sorting efficiency of 2028 picks/h is not as high as some prior methods. We focus on the detection system because it provides the greatest opportunity for improved sorting efficiency through the utilization of myriad well-developed robotic techniques, in particular, in the capture path and ordering of the robot.

Acknowledgements This work was supported by the Research and industrialization on Key Technologies of mobile construction waste recycling [Grant Number 2018C001]; the Research and industrialization on key technology of quality inspection of machine-made sand form [Grant Number 2019G003]; the Research on the joint development and industrialization of key technologies of large capacity full hydraulic cone crusher [Grant Number 2018I1006]; and the Subsidized Project for Postgraduates' Innovative Fund in Scientific Research of Huaqiao University. And we thank Adam Przywecki, B.Eng., from Liwen Bianji, Edanz Editing China (www.liwenbianji.cn/ac) and Berenice (www.enago.cn), for editing the English text of a draft of this manuscript.

Funding This study was funded by the Research and industrialization on Key Technologies of mobile construction waste recycling (Grant Number 2018C001); the Research and industrialization on key technology of quality inspection of machine-made sand form (Grant Number 2019G003); the Research on the joint development and industrialization of key technologies of large capacity full hydraulic cone crusher (Grant Number 2018I1006) and the Subsidized Project for Postgraduates' Innovative Fund in Scientific Research of Huaqiao University.

Compliance with ethical standards

Conflict of interest The authors declare that they have no conflict of interest.

References

- Cesetti M, Nicolosi P (2016) Waste processing: new near infrared technologies for material identification and selection. *J Instrum.* <https://doi.org/10.1088/1748-0221/11/09/C09002>
- Chen T, He Y (2018) Research on treatment process of decorative construction waste. In: IOP conference series: materials science and engineering. <https://doi.org/10.1088/1757-899x/394/5/052018>
- Chin L, Lipton J, Yuen MC, Bottiglio RK, Rus D (2019) Automated recycling separation enabled by soft robotic material classification. In: 2019 2nd IEEE international conference on soft robotics (RoboSoft). <https://doi.org/10.1109/ROBOSOFT.2019.8722747>
- Diya SZ, Proma RA, Islam MN, Anannya TT, Mamun AA, Arefeen R, Mamun SA, Rahman II, Rabbi MF (2018) Developing an intelligent waste sorting system with robotic arm: a step towards green environment. In: 2018 international conference on innovation in engineering and technology (ICIET). <https://doi.org/10.1109/CIET.2018.8660890>
- Gomes OFM, Lima PRL (2010) Classification of fine particles from construction and demolition waste through image analysis. In: IWSSIP 2010–17th international conference on systems, signals and image processing
- Huang GB (2014) An insight into extreme learning machines: random neurons, random features and kernels. *Cognit Comput* 6:376–390. <https://doi.org/10.1007/s12559-014-9255-2>
- Huang B, Wang X, Kua H, Geng Y, Bleischwitz R, Ren J (2018) Construction and demolition waste management in China through the 3R principle. *Resour Conserv Recycling* 129:36–44. <https://doi.org/10.1016/j.resconrec.2017.09.029>
- Kujala JV, Lukka TJ, Holopainen H (2016) Classifying and sorting cluttered piles of unknown objects with robots: a learning approach. <https://doi.org/10.1109/IROS.2016.7759167>
- Mauruschat D, Plinke B, Aderhold J, Gunschera J, Meinihschmidt P, Salthammer T (2016) Application of near-infrared spectroscopy for the fast detection and sorting of wood–plastic composites and waste wood treated with wood preservatives. *Wood Sci Technol* 50:313–331. <https://doi.org/10.1007/s00226-015-0785-x>
- Nowakowski P, Pamuta T (2020) Application of deep learning object classifier to improve e-waste collection planning. *Waste Manag* 109:1–9. <https://doi.org/10.1016/j.wasman.2020.04.041>
- Paranhos R, Cazacliu B, Sampaio C, Petter C, Neto R, Huchet F (2016) A sorting method to value recycled concrete. *J Clean Prod* 112:2249–2258. <https://doi.org/10.1016/j.jclepro.2015.10.021>
- Paulraj SG, Hait S, Thakur A (2016) Automated municipal solid waste sorting for recycling using a mobile manipulator. In: International design engineering technical conferences and computers and information in engineering conference. vol 50152. American Society of Mechanical Engineers. <https://doi.org/10.1115/DETC2016-59842>
- Paulraj S, Hait S, Thakur A (2017) Multi-material classification of dry recyclables from municipal solid waste based on thermal imaging. *Waste Manag* 70:13–21. <https://doi.org/10.1016/j.wasman.2017.09.019>
- Rutkowski L, Jaworski M, Pietruszuk L, Duda P (2014) The CART decision tree for mining data streams. *Inf Sci* 266:1–15. <https://doi.org/10.1016/j.ins.2013.12.060>
- Sarc R, Curtis A, Kandlbauer L, Khodier K, Lorber KE, Pomberger R (2019) Digitalisation and intelligent robotics in value chain of circular economy oriented waste management—a review. *Waste Manag* 95:476–492. <https://doi.org/10.1016/j.wasman.2019.06.035>
- Serranti S, Gargiulo A, Bonifazi G (2012) Classification of polyolefins from building and construction waste using NIR hyperspectral imaging system. *Resour Conserv Recycl* 61:52–58. <https://doi.org/10.1016/j.resconrec.2012.01.007>
- Toğacıar M, ErgenB Cömert Z (2020) Waste classification using AutoEncoder network with integrated feature selection method in convolutional neural network models. *Measurement* 152:107459. <https://doi.org/10.1016/j.measurement.2019.107459>
- Ulsen C, Kahn H, Hawlitschek G, Masini EA, Angulo SC (2013) Separability studies of construction and demolition waste recycled sand. *Waste Manag* 33:656–662. <https://doi.org/10.1016/j.wasman.2012.06.018>
- Wu X, Li J, Yao L, Xu Z (2020) Auto-sorting commonly recovered plastics from waste household appliances and electronics using near-infrared spectroscopy. *J Clean Prod*. <https://doi.org/10.1016/j.jclepro.2019.118732>
- Xiao W, Yang J, Fang H, Zhuang J, Ku Y (2019) A robust classification algorithm for separation of construction waste using NIR hyperspectral system. *Waste Manag* 90:1–9. <https://doi.org/10.1016/j.wasman.2019.04.036>

Publisher's Note Springer Nature remains neutral with regard to jurisdictional claims in published maps and institutional affiliations.

Terms and Conditions

Springer Nature journal content, brought to you courtesy of Springer Nature Customer Service Center GmbH (“Springer Nature”). Springer Nature supports a reasonable amount of sharing of research papers by authors, subscribers and authorised users (“Users”), for small-scale personal, non-commercial use provided that all copyright, trade and service marks and other proprietary notices are maintained. By accessing, sharing, receiving or otherwise using the Springer Nature journal content you agree to these terms of use (“Terms”). For these purposes, Springer Nature considers academic use (by researchers and students) to be non-commercial.

These Terms are supplementary and will apply in addition to any applicable website terms and conditions, a relevant site licence or a personal subscription. These Terms will prevail over any conflict or ambiguity with regards to the relevant terms, a site licence or a personal subscription (to the extent of the conflict or ambiguity only). For Creative Commons-licensed articles, the terms of the Creative Commons license used will apply.

We collect and use personal data to provide access to the Springer Nature journal content. We may also use these personal data internally within ResearchGate and Springer Nature and as agreed share it, in an anonymised way, for purposes of tracking, analysis and reporting. We will not otherwise disclose your personal data outside the ResearchGate or the Springer Nature group of companies unless we have your permission as detailed in the Privacy Policy.

While Users may use the Springer Nature journal content for small scale, personal non-commercial use, it is important to note that Users may not:

1. use such content for the purpose of providing other users with access on a regular or large scale basis or as a means to circumvent access control;
2. use such content where to do so would be considered a criminal or statutory offence in any jurisdiction, or gives rise to civil liability, or is otherwise unlawful;
3. falsely or misleadingly imply or suggest endorsement, approval , sponsorship, or association unless explicitly agreed to by Springer Nature in writing;
4. use bots or other automated methods to access the content or redirect messages
5. override any security feature or exclusionary protocol; or
6. share the content in order to create substitute for Springer Nature products or services or a systematic database of Springer Nature journal content.

In line with the restriction against commercial use, Springer Nature does not permit the creation of a product or service that creates revenue, royalties, rent or income from our content or its inclusion as part of a paid for service or for other commercial gain. Springer Nature journal content cannot be used for inter-library loans and librarians may not upload Springer Nature journal content on a large scale into their, or any other, institutional repository.

These terms of use are reviewed regularly and may be amended at any time. Springer Nature is not obligated to publish any information or content on this website and may remove it or features or functionality at our sole discretion, at any time with or without notice. Springer Nature may revoke this licence to you at any time and remove access to any copies of the Springer Nature journal content which have been saved.

To the fullest extent permitted by law, Springer Nature makes no warranties, representations or guarantees to Users, either express or implied with respect to the Springer nature journal content and all parties disclaim and waive any implied warranties or warranties imposed by law, including merchantability or fitness for any particular purpose.

Please note that these rights do not automatically extend to content, data or other material published by Springer Nature that may be licensed from third parties.

If you would like to use or distribute our Springer Nature journal content to a wider audience or on a regular basis or in any other manner not expressly permitted by these Terms, please contact Springer Nature at

onlineservice@springernature.com